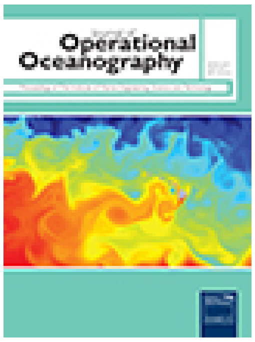

Taylor & Francis
Taylor & Francis Group

Journal of Operational Oceanography

ISSN: 1755-876X (Print) 1755-8778 (Online) Journal homepage: http://www.tandfonline.com/loi/tjoo20

Getting the right wind-forcing for an ecosystem model: A case study from the eastern Arabian Sea

Kunal Chakraborty , Nimit Kumar & G. V. M. Gupta

To cite this article: Kunal Chakraborty , Nimit Kumar & G. V. M. Gupta (2017): Getting the right wind-forcing for an ecosystem model: A case study from the eastern Arabian Sea, Journal of Operational Oceanography, DOI: 10.1080/1755876X.2017.1354686

To link to this article: http://dx.doi.org/10.1080/1755876X.2017.1354686

Published online: 31 Jul 2017.

JOURNAL OF OPERATIONAL OCEANOGRAPHY, 2017
https://doi.org/10.1080/1755876X.2017.1354686

Getting the right wind-forcing for an ecosystem model: A case study from the eastern Arabian Sea

Kunal Chakraborty [a], Nimit Kumar [a] and G. V. M. Gupta [b]

[a]Indian National Centre for Ocean Information Services, Hyderabad, India; [b]Ministry of Earth Sciences, Centre for Marine Living Resources and Ecology, Kochi, India

ABSTRACT
The state of the ocean simulated through a numerical model is extremely sensitive to the forcing and hence, the choice of appropriate forcing is essential, in particular wind-fields. We compared Regional Ocean Modeling System (ROMS) simulations when forced with two different wind-fields derived from satellite sensors (scatterometers), namely QuickSCAT and ASCAT, while keeping the remaining configurations the same. This study had been carried out during the operational overlapping period of these scatterometers (2007–2009). We observed that the simulations of upper ocean chlorophyll distribution and depth of sub-surface chlorophyll maximum were vastly diverging when the model was forced with different scatterometer forcings. In order to determine which of the forcings yielded coastal productivity closer to observations, we compared model-simulated upper ocean chlorophyll concentration with *in situ* observations along the eastern Arabian Sea. For all the sub-regions, the QuickSCAT wind-forced coastal productivity was better correlated with *in situ* chlorophyll than its counterpart. However, this signature was most prominent in the wind-driven upwelling regime of the south-eastern Arabian Sea. Additionally, when compared with surface chlorophyll derived from SeaWiFS and MODIS-Aqua satellites, we found that the QuickSCAT simulated interannual variability was in better agreement in comparison to its counterpart.

ARTICLE HISTORY
Received 1 August 2016
Accepted 23 June 2017

KEYWORDS
ROMS; scatterometer; QuickSCAT; ASCAT; chlorophyll; SeaWiFS; MODIS-Aqua

1. Introduction

In the past few decades, ocean colour satellite remote sensing has yielded a wealth of knowledge pertaining to the productivity trends in the oceans. However, satellite data have limitations, namely resolving data for the night side of the earth and unable to provide profile of the ocean water column. Moreover, data availability is restricted to the presence of the clouds. Biogeochemical models coupled with ocean general circulation models can offer a solution to these data limitations. Such numerical models can simulate the transport of water-mass packets across the pre-defined layers and grid-cells. Size of these layers and grid-cells defines vertical and horizontal resolution of the output, respectively. Additionally, numerical models allow the user to define the frequency at which the outputs are to be generated. A fine-tuned model with continuous assimilation of recent observations tends to simulate real-world conditions on the satisfactory levels for operational needs (Penny et al. 2015). The outputs do not have spatial or temporal data gaps. Moreover, instantaneous vertical profiles or time evolution of a feature across the water column can be captured for research or operational purposes.

The primary requirement of a numerical ocean model to simulate the state of the ocean is forcing that a real-world ocean experiences. Once the model is defined, surface winds provided from the observation or model play a crucial role in achieving realistic perturbations in otherwise steady-state of the ocean (Burillo et al. 2002; Maltrud and McClean 2005). Winds tend to displace warmer water-mass on the surface (by lateral advection) and allow cooler waters to rise to the surface from below. This reduces the temperature difference within the water column, triggering mixing up to deeper layers. Such a mixing will result in colder sea surface temperature, deeper thermocline and mixed layer depth (MLD), and elevated nutrient concentrations resulting in enhanced phytoplankton production (Ravichandran et al. 2012). Therefore, a well-behaved model should, in theory, yield upwelling and productivity signatures akin to observations. However, this is subject to the availability of observed local as well as remote wind-forcing in a specified area of interest.

CONTACT Kunal Chakraborty kcincoishyb@gmail.com Indian National Centre for Ocean Information Services, Ocean Valley, Pragathi Nagar (BO), Nizampet (SO), Hyderabad, India

Thus, a coupled physical–biogeochemical model should have an appropriate wind-forcing to provide reliable output. Usually this is achieved by utilising satellite-derived wind-fields due to their vast and unmatchable spatio-temporal coverage. Therefore, the source and quality of wind-field along with its period become of utmost importance for the model to perform well. Models are required to spin for many years, often for decades, but the life-span of a satellite lasts only for a few years. If the sensor onboard the successor satellite is the same, transition from one dataset to another can be seamless. If not, an overlap period may be used for ensuring that the forcing does not affect model sensitivity. Such a transition occurred between different scatterometers onboard QuickSCAT and ASCAT satellites with an overlap period of two years during 2007–2009 (Bentamy et al. 2012; Bentamy and Fillon 2012). Comparative studies have been attempted for the Indian Ocean and elsewhere, to validate sensors against the observations as well as to evaluate outputs of the physical models that use wind-field derived from these two satellites (Schlax et al. 2001; Bentamy et al. 2008, 2012; Bourassa et al. 2010; Sivareddy et al. 2013, 2015). These studies found that ASCAT performs better in low-wind speed conditions, whereas QuickSCAT can resolve higher wind-speed conditions better. However, there are no biogeochemical model studies for the Indian Ocean that attempts such a comparison with different wind-forcings.

The northern Indian Ocean has a unique biogeochemistry. It is a result of being land-locked in the north, due to which the northern extent is in the tropic. The seasonality of reversing monsoonal winds profoundly influences the biogeochemistry of this region (Webster et al. 1999). The Indian summer monsoon (ISM or southwest monsoon) prevails from June to September, whereas the Indian winter monsoon (IWM or northeast monsoon) spans from December to February. The ISM is associated with the low-level atmospheric strong Somali jet winds towards the Indian subcontinent, which reverses in the IWM although with a lower magnitude. The intermonsoon periods are characterised by low wind magnitude and reversal of the direction. The western Arabian Sea (AS) is adjacent to the horn of Africa and the Arabian Peninsula, and this region experiences high atmospheric pressure most part of the year. This results in the aeolian transport (referred to as the *Shamal* activity) to the basin as well as persistent upwelling in the off-Somalia region and along the coast of Yemen during ISM (Rao et al. 2001, 2003; Preusser et al. 2002; Singh et al. 2008). Enhanced plankton biomass resulting from wind-driven upwelling in this region is advected towards the central AS (Keen et al. 1997).

Winter convective mixing is another physical phenomenon that uplifts deeper cooler and nutrient-rich waters to upper ocean in the northern AS, which result in blooming of phytoplankton during early spring bloom (February–March) (Madhupratap et al. 2001; Prasanna Kumar et al. 2001; Menon et al. 2006). Following the equatorward west India coastal current, the resultant spring bloom water-mass is subsequently transported southerly along the eastern AS (EAS). Decomposition of this large sinking biogenic flux results in the development of a persistent oxygen minimum zone (OMZ) extending from north to central AS thereby resulting in large net-export of CO_2 to the atmosphere (Sarma et al. 1998; Naqvi et al. 2000; Prasanna Kumar et al. 2001). The horizontal expansion of OMZ occurs as upwelling influences the coastal productivity during ISM (Devol et al. 2006; Sudheesh et al. 2016). Monsoonal reversal of winds and in turn coastal currents, along with high amount of river discharges generate high degree of variability in the productivity induced from either mixing or upwelling, in the EAS (Sarupria and Bhargava 1993; Madhupratap et al. 2001; Srinivas and DineshKumar 2006; Habeebrehman et al. 2008; Jayaram et al. 2010; Chauhan et al. 2011; Joshi and Rao 2012; Gupta et al. 2016; Sudheesh et al. 2016). This underlines that the AS is an ideal laboratory to study the impact of forcing in simulating the ecosystem processes responsible for the variability in coastal productivity.

In this study, for the first time, we attempt to compare the biogeochemical model outputs in terms of chlorophyll concentration using wind-fields derived from two scatterometers – QuickSCAT and ASCAT – for the operational overlap period of the years 2007–2009. We also attempt to find potential reasons for difference in the biological outputs.

2. Study area

In this work, we focus on biophysical simulation of the EAS while addressing northern, central and southern regions of EAS as separate case studies owing to their distinct characteristics (Figure 1).

The northern EAS (NEAS) witnesses a short ISM, no effects from IWM, bears widest continental shelf (CS) and supports large spring blooms (Madhupratap et al. 2001; Prasanna Kumar et al. 2001; Menon et al. 2006). This region witnesses two chlorophyll peaks during a year. The high chlorophyll episode in the ISM is a precursor of coastal upwelling, whereas another episode with maximum surface Chl*a* occurs in the IWM due to convective mixing.

The central EAS (CEAS) is influenced by ISM and IWM as well as discharge from multiple rivers (Shetye et al. 1995; Qasim 2003; Menon et al. 2005, 2011). These regions also recurrently witness spring bloom of *Trichodesmium* spp. This, along with coastal current dynamics, upwelling and high rainfall ensure high coastal productivity with elevated surface chlorophyll values up to 32–39 mg m^{-3} off Mangalore (Madhupratap et al. 2001; Jayram et al. 2010; Raghavan et al. 2010; Chauhan et al. 2011; Sudheesh et al. 2016).

The southern EAS (SEAS) has narrower CS compared to the CEAS and is also influence by ISM and IWM. SEAS also experiences high photic column chlorophyll (~40 mg m^{-2}) and net primary production (~1300 mgC m^{-2} d^{-1}) off Kochi during summer upwelling (Gupta et al. 2016). Coastal waters off Kochi also show extreme seasonal variability in productivity between ISM (40–1225 mgC m^{-2} d^{-1}), post-ISM 21–263 mgC m^{-2} d^{-1}) and during the intermonsoon period (12–648 mgC m^{-2} d^{-1}) (Sarupria and Bhargava 1993; Srinivas and Dinesh-Kumar 2006; Habeebrehman et al. 2008; Jayaram et al. 2010; Joshi and Rao 2012; Gupta et al. 2016).

3. Data and methods

3.1. Satellite data

3.1.1. QuickSCAT

QuickSCAT was a NASA (National Aeronautics and Space Administration) polar-orbiting satellite having the 'SeaWinds' (though, often referred to as QuickSCAT sensor) Ku-band scatterometer, that served from June 1999 to November 2009, thereafter its antenna rotation malfunctioned. Data were collected on either (day/night) side of the earth, segregated as ascending and descending pass data. It provided data at high spatial and temporal resolutions with 1800 km swath, covering around 90% of oceans daily at 25 km^2 resolution. We used QuickSCAT wind-fields from ftp://ftp.ifremer.fr/ifremer/cersat/products/gridded/MWF/L3/ data portal at daily temporal scale and ~25 km of spatial resolution.

3.1.2. ASCAT

ASCAT (Advanced Scatterometer) is a C-band scatterometer that has been deployed so far onboard MetOp series polar-orbiting satellites by EUMETSAT (European Meteorological Satellite Organization). A Ku-band variant has been also deployed onboard Oceansat-2 by ISRO (Indian Space Research Organization). However, for the period of this comparative study (i.e. 2007–2009) data from ASCAT onboard MetOp-A (aka MetOp-2) were only available. It provided ascending as well as descending pass data at 25 km^2 resolution, over two 550 km swath on either side of the ground track, with the help of three fixed antennas for each swath (one perpendicular to the ground track and remaining at ±45° to the fore and to the aft). We used ASCAT wind-fields from ftp://ftp.ifremer.fr/ifremer/cersat/products/gridded/MWF/L3/ data portal at daily temporal scale and 25 km of spatial resolution.

3.1.3. Satellite chlorophyll data

We used SeaWiFS (Sea-viewing Wide Field-of-view Sensor) satellite's 8-day averaged chlorophyll data product with 10 km spatial resolution from NOAA (National Oceanic and Atmospheric Administration) CoastWatch data portal. Similar data product of NASA's MODIS (Moderate-resolution Imaging Spectroradiometer) series satellite Aqua was also obtained. Further details for SeaWiFS and Aqua missions are provided on the OceanColor portal by NASA's Goddard Space Flight Center (GSFC). These data were normalised to match spatial resolution of the model for comparison.

3.2. Model description

The INCOIS coupled biophysical model is composed of a three-dimensional ocean circulation model, ROMS (Regional Ocean Modelling System) version 3.6 (Haidvogel et al. 2008), and a biological model consisting of the nitrogen cycle model containing parameterised sediment denitrification as described in Fennel et al. (2006), and a carbonate chemistry component following Zeebe and Wolf-Gladrow (2001). The ROMS model was set up for the entire Indian Ocean basin from 30°E to 120°E in the east–west direction and 30°S to 30°N in the north–south direction. The model has a horizontal resolution of 0.25° and has 40 sigma levels in the vertical. The vertical profile has a resolution of 0.7 m nearshore. Off the shelf to a bottom depth of 5000 m, the vertical resolution ranges from 15 m at the surface to 500 m at the bottom. The bathymetry is supplied by Sindhu et al. (2007). The vertical constraint parameters are selected so as to reproduce fine scale vertical resolution for the upper ocean. There are approximately 26 levels in the top 200 m of the water column in the deep ocean (with a depth >3500 m). In the shallower regions, the number of levels in the water column is increased. The K-Profile Parameterisation (Large et al. 1994) vertical mixing scheme is used. Biharmonic viscosity and diffusion schemes are chosen for horizontal mixing. The lateral boundaries in the east and south are treated as open. The western and northern boundaries are solid walls. It is challenging to configure high-resolution global models due to computational limitations. A global model with coarse resolution fails to capture fine scale variabilities in the regional oceans. In order to overcome these difficulties, we adopted the one-way nested modelling approach in which a global ocean general circulation model provides boundary information to a regional model that is further coupled to an ecosystem model (Shulman et al. 2003). This approach utilises strong relaxation at the open boundaries, but weaker relaxation in shallow waters and productive zones to allow the model to respond more freely to surface atmospheric forcing.

The model was spun up for a period of 10 years from an initial state derived from the monthly climatological values of January of all the prognostic variables of the physical state of the ocean estimated from Estimating the Circulation and Climate of the Ocean (ECCO) data. The model was forced using climatological winds and fluxes derived, respectively, from QuikSCAT and objectively analysed flux (OAux) data (Lisan et al. 2008) during the spin-up time. Then the biological module is switched on. Nitrogen and oxygen, however, were initialised using the World Ocean Atlas 2009 data. Due to lack of any information on the spatial distribution of other biological state variables in the Indian Ocean, the initial states of these biological variables were set uniformly throughout the ocean at 0.01 mg m^{-3} in the hope that given sufficient time the transient processes will decay and coupled dynamics in the model will be able to capture the salient spatio-temporal features of these variables. The three-dimensional momentum and tracer fields were clamped at the eastern and southern boundary to the monthly climatological values derived from ECCO. However, the model uses a Flather (1976) boundary condition for the free surface and Chapman (1985) boundary conditions on the two-dimensional momentum fields. Closed boundary conditions were used for the biological variables knowing that the number of observations of biogeochemical variables is limited in and around the Indian Ocean. Clamped boundary conditions were used for nitrogen and oxygen.

The climatological run was carried out for the coupled set-up for 30 years after which the model was forced with realistic atmospheric data in order to simulate the true state of the ocean. QuikSCAT and ASCAT winds were used to force the model, respectively, during the period of 1 January 2000 to 18 November 2009 and 2 April 2007 to 31 December 2012. The OAflux data were used to compute the air–sea fluxes (surface air temperature, surface specific humidity, net longwave radiation and net shortwave radiation) required to force the model. The physical variables were initialised with the state of the ocean as available in the ECCO on 1 January 2000 during the interannual run. The biological variables were initialised using the climatological state of January generated during climatological run of the coupled set-up. Thus, the processes and features resolved at larger scales are percolated through the boundaries of the Indian Ocean grid and should have a major impact on the interior dynamics of the system. There was an overlap period of two years (2007–2009) when both the sensors were operational. Daily model outputs were extracted from both the simulations between 2 April 2007 and 18 November 2009 for the validation and time-series analysis.

3.3. In situ *observations*

In situ data on chlorophyll for the years 2007–2009 all along the EAS (within the Indian Exclusive Economic Zone; Figure 1) were obtained from various cruises onboard FORV Sagar Sampada as part of the observations made under Marine Living Resources Program of Ministry of Earth Sciences, India. In brief, 1–2 L of seawater, collected from various depths through Niskin bottles attached to the CTD profiler, was filtered using Whatman GF/F filter under gentle vacuum and Chlorophyll *a* was measured spectrophotometrically following the 90% acetone extraction method (Parsons et al. 1984). The collated data showed that almost the entire sampling is confined to standard depths (0, 10, 20, 30, 50, 100 and 120 m) due to non-availability of the fluorescence sensor attached to the CTD profiler. This probably ends up in variation between the actual depth of sub-surface chlorophyll maxima and the depth of sampling maxima, which is a limitation in this study. The data also showed high density of sampling in the SEAS (Figure 1) especially during spring intermonsoon (April) and summer monsoon (June–September; upwelling period) which are phytoplankton bloom seasons. Compared to SEAS, sampling density in the CEAS was relatively less although similar seasonal blooms were also encountered in this region. NEAS was least sampled among all the three regions and the sampling was more during winter (November–January) and early spring (February–April) seasons owing to the formation of winter convective mixing blooms. Temperature profiles from an Argo-float (WMO ID 2900776) deployed in the south-central AS (Figure 1) was used for the validation of model-simulated temperature in the upper ocean. Additionally, the Geostrophic and Ekman Current Observatory (GEKCO) product (developed by Joël Sudre at LEGOS, France) was used to validate the surface currents. This product provides Zonal (u) and Meridional (v) component of the surface current data at quarter degree spatial resolution and was obtained from the resulting GEKCO (Sudre and Garçon 2013).

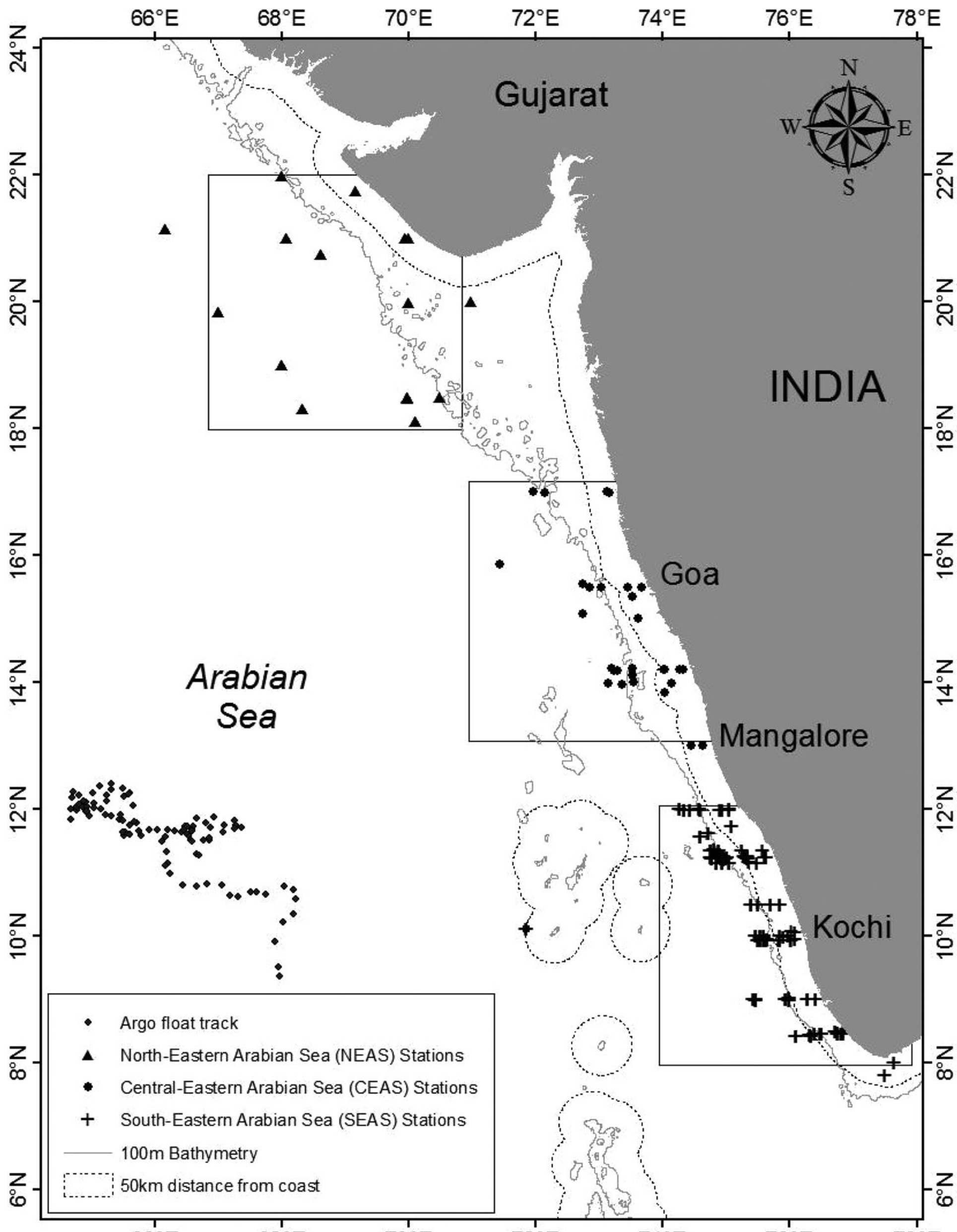

Figure 1. Study area with Argo-float track (in south-central AS) and *in situ* sampling locations (along the coastal EAS) used for comparing model outputs and extents (rectangles) used for model and satellite data inter-comparison.

4. Results and discussion

4.1. Validation of the model hydrodynamics

In order to ensure that the model is able to capture the reliable hydrodynamics of the region, we compared the simulations of the models (forced with both the wind-fields) with observations. The mixing of the upper ocean is determined by the density gradient across the seawater column. Based on the equation of state, this can either be dominated by temperature or salinity of the water column (Pickard and Emery 1990). Accordingly, the density in this region mostly depends on temperature. We compared *in situ* temperature profiles collected by an Argo-float (Figure 1) with the model simulations along the same track (Figure 2). Both the models were found to capture the seasonal cycles effectively, including deeper MLD during summer monsoon and the shoaling of the thermocline during post summer monsoon.

The comparison of model-simulated climatological surface currents with GEKCO surface current climatology along the west coast of India is shown in Figure 3. Additionally, in order to validate the seasonality observed in the AS, we made this comparison on seasonal scale. The model is well in agreement with the observed seasonally reversing alongshore currents:

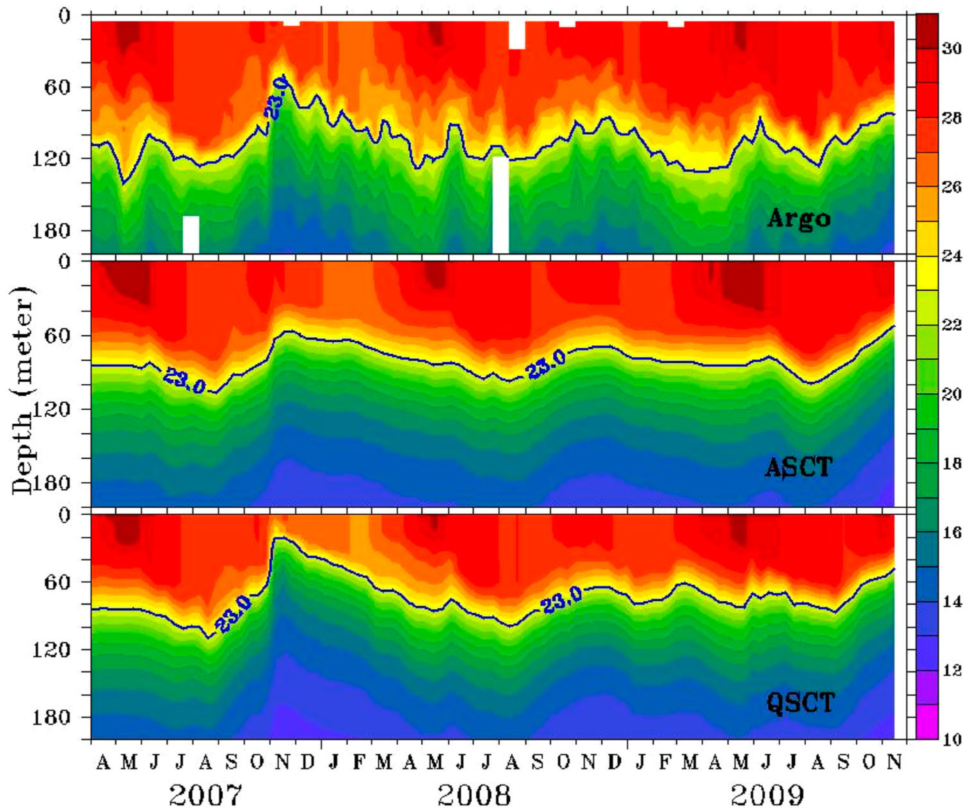

Figure 2. Comparison of Argo-float temperature (°C) profiles with along-track profiles from identical ROMS biophysical numerical ocean models forced separately by ASCAT (ASCT) and QuickSCAT (QSCT) wind-fields.

upwelling favoured equatorward flow during summer (JJAS) and poleward flow during winter (ON and DJF) (Amol et al. 2012). A basin-wide anti-cyclonic gyral circulation starts to appear sometime in May in the AS; as a result the currents along the west coast of India flow equatorward. This is the only time when circulation in the eastern boundary of the AS looks similar to the typical eastern boundary currents in the tropics (Shetye and Shenoi 1988). As summer progresses, the strength of the equatorward current increases and reaches its peak during August–September. However, the strength and the spread of this boundary current are not the same throughout along the west coast, but is weak and much broader in the north, whereas strong and narrower in the south.

We also observed that models forced by both the wind-forcings were capable of capturing geographically significant trends across the AS basin. This includes the stronger currents due to persistent upwelling off Somalia, and monsoonal current in the south-central AS as well as off southwest coast of India.

4.2. Inter-comparison of model outputs

We extracted various physical column properties and chlorophyll concentration averaged over the sub-regions (Figure 1), along the EAS for the period April 2007–November 2009 (Figure 4) (Prakash et al. 2012; Tilstone et al. 2013; Chakraborty et al. 2016). We observed that wind-fields from QuickSCAT and ASCAT were able to introduce significant perturbations in our numerical model. The wind-forcings allowed the mixing over the upper ocean to deepen the MLD. However, the degree of wind-induced mixing in all the sub-regions was inherently different between the two models (Figure 4). QuickSCAT-induced forcing was able to generate a higher degree of mixing and thereby facilitating entrainment of nutrients from the below mixed layer and enhancing productivity, which varied latitudinally (Figure 4). The difference in the magnitude of productivity between the wind-forcings was the highest in the SEAS and decreased towards the northern sub-regions. The southwest monsoonal winds influence strong upwelling in the SEAS (Chakraborty et al. 2016) as it generates a northward propagating upwelling Kelvin wave along the west coast. This indicates that for the areas and seasons where wind-induced mixing or upwelling is the prime contributor to productivity, forcing becomes an important factor for simulation.

As all the parameters and boundary conditions other than wind-forcings were kept the same in the model, this can be considered an ideal case of sensitivity analysis. By

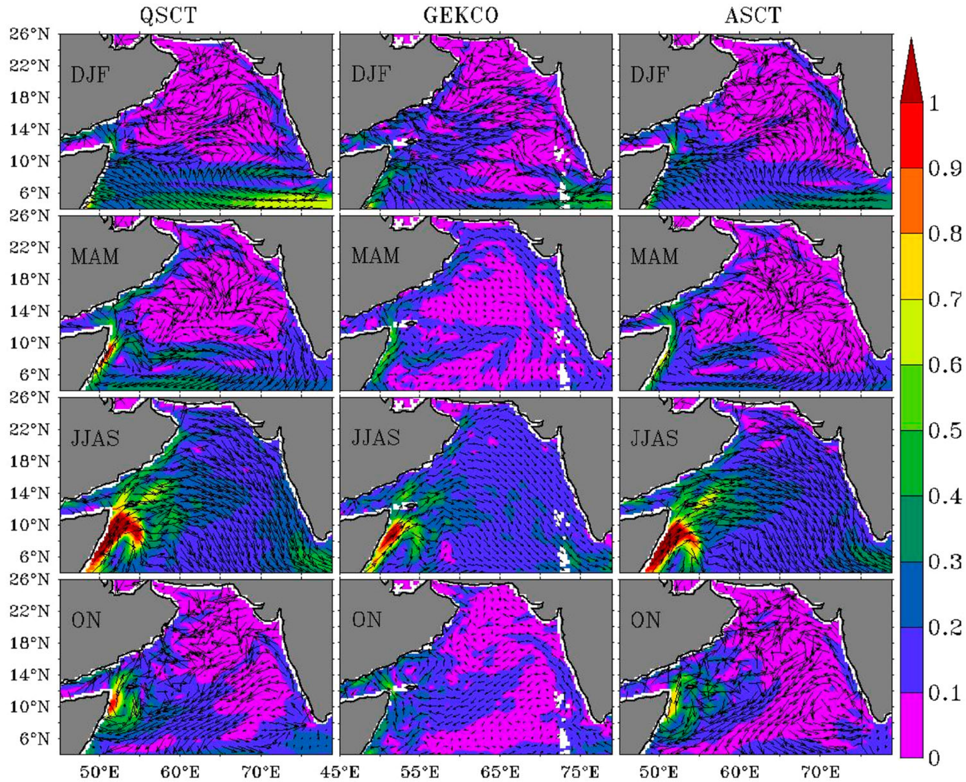

Figure 3. Comparison of seasonal mean surface currently derived from GEKCO (Obs) with those derived from identical ROMS biophysical ocean models forced separately by ASCAT (ASC) and QuickSCAT (QSC) wind-fields. Colour shading shows the magnitude while the vectors (of fixed length) show the direction, of the surface currents.

this procedure, given similar light and nutrient availability in the deeper waters as initial conditions, wind-induced mixing primarily plays a pivotal role in modulating the upper ocean productivity. This is clearly seen through the deepening of MLD that permits nutrient entrainment in the mixed layer and its subsequent upward contraction enhances chlorophyll concentration (Figure 4). This shows higher the deepening of MLD and further its contraction, higher the productivity that can be observed. QuickSCAT forcing was found to oscillate the MLD more efficiently than its counterpart, therefore resulting in relatively higher productivity.

Apart from magnitude, another effect from wind-induced forcing is the depth at which a model simulates chlorophyll maxima. Vertical movement of thermocline or MLD over the time determines at what depth chlorophyll maxima is generated in a numerical model. Recent studies of Gupta et al. (2016) from SEAS shelf have reported chlorophyll maximum at surface associated with shallow MLD during summer upwelling and its depth deepens with the deepening of the MLD during rest of the year. These trends are very well captured by the model with both the wind-fields (Figure 4). However, despite generating a similar trend for depth of chlorophyll maxima, its magnitude varies between these outputs and regions.

To address such spatial variability arising from the regional factors, we calculated difference in SCM_{Depth} between both the model outputs across the EAS (Figure 5). We calculated this for the months of January and July in order to study seasonal extremes (winter and summer monsoon, respectively). The positive values indicate that chlorophyll maxima simulated by the QuickSCAT forced model was deeper than the one simulated with the ASCAT forced model, and vice versa.

We observed that in coastal EAS, QuickSCAT winds induced shallower SCM_{Depth} (negative values, purple-blue, Figure 5) in comparison to ASCAT winds, whereas the signature was opposite for the parts of central AS. The same trend was significant during summer monsoon (QuickSCAT) to winter monsoon (ASCAT) and its latitudinal variability. QuickSCAT yield of shallower chlorophyll maxima was found to be dominated more towards SEAS while at small expanses, ASCAT wind-derived chlorophyll maxima were often seen closer to the surface in the NEAS. As the basin scale simulation of surface currents fared well in comparison to the observations (Figure 3), we infer that such trends are the derivative of local processes. In order to check which of these forcings yield more realistic scenario, we compared outputs with *in situ* as well as satellite-based observations.

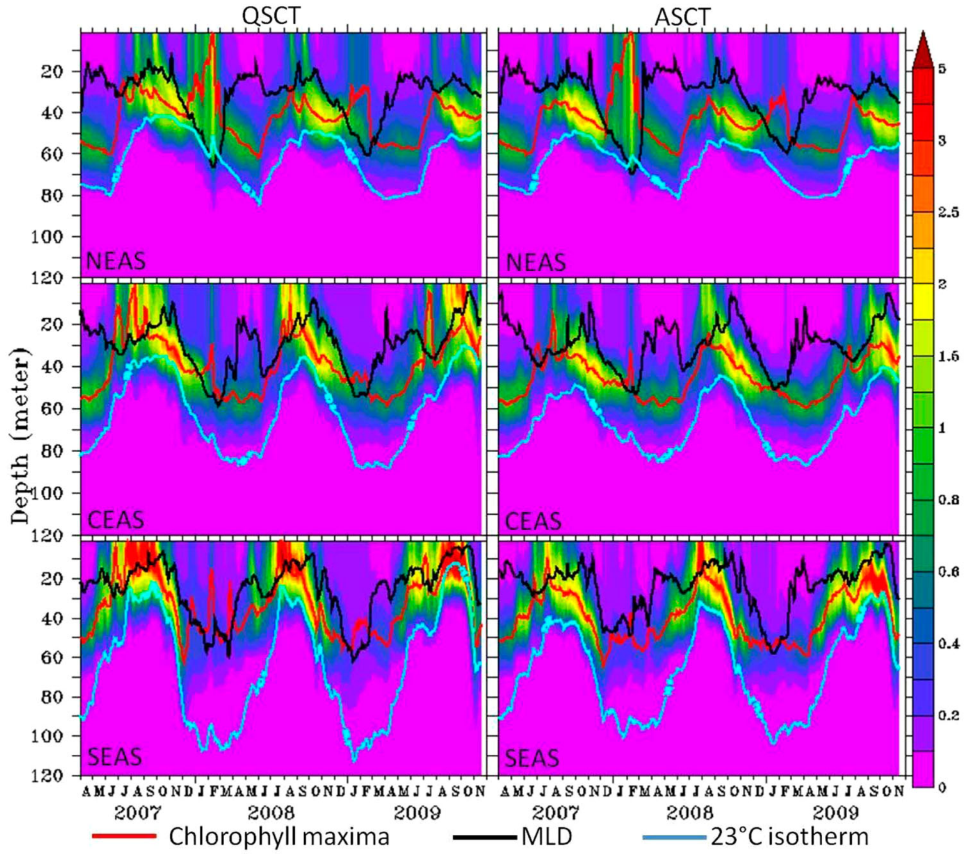

Figure 4. Comparison of model-simulated biophysical variables (averaged across the sub-regions or boxes shown in Figure 1) derived from identical ROMS biophysical ocean models forced separately by QuickSCAT and ASCAT wind-fields.

4.3. Comparison of model outputs with in situ observations

While inter-comparison gave us indication towards relative performance between the forcings, it is also required to study the performance relative to the *in situ* observations. We used chlorophyll profiles measured along the EAS over different seasons for the study period. It is important to note that *in situ* data have been collected at standard depths which may differ from actual depth of sub-surface chlorophyll maxima (SCM_{Depth}). In general, the SCM_{Depth} varies with season and region; it occupies within upper 30 m during productive periods, but deepens up to ~60 m during the less productive period. Following this general trend, high density of *in situ* data was found within upper 50 m with 10 m sampling interval. Even in cases where the actual SCM_{Depth} falls within this standard depth interval of 10 m, the deviation would not exceed ±5 m. So, the same is considered as an acceptable limit of model error.

The physical and biogeochemical dynamics along coastal EAS varies with region. This leads to variability in magnitude of production, depth of maximum, seasonality between these sub-regions. The model produced outputs of both wind-field forcings at different depth layers corresponding to *in situ* data that have been used for comparison. A cap of ±90% bias was applied to either of the simulations and extreme bias outliers were removed. The survivor data-points were then used for linear regression for both the forcings' outputs.

4.3.1. NEAS

Out of 105 match-up data-points, only a fraction (≈10%) had an exact match. After applying a threshold of ±90% bias, 86 data-points remained. The correlation of the same showed that the outputs of the model forced with QuickSCAT wind-fields provided a better match with *in situ* chlorophyll than that of the model forced with ASCAT wind-field; despite both the model forcings having largely underestimated the chlorophyll concentration (Figure 6). Indeed, among the QuickSCAT forced simulations in all three sub-regions (Figure 6) NEAS showed least correlation. This shows that processes governing productivity in this region do not rely mainly on the wind-induced mixing or upwelling. Upwelling in the NEAS is the weakest of all the regions, as inferred from the lowest chlorophyll concentrations during peak summer monsoon (July–August; Figure 4), indicating the weak role of winds. Winter convective mixing

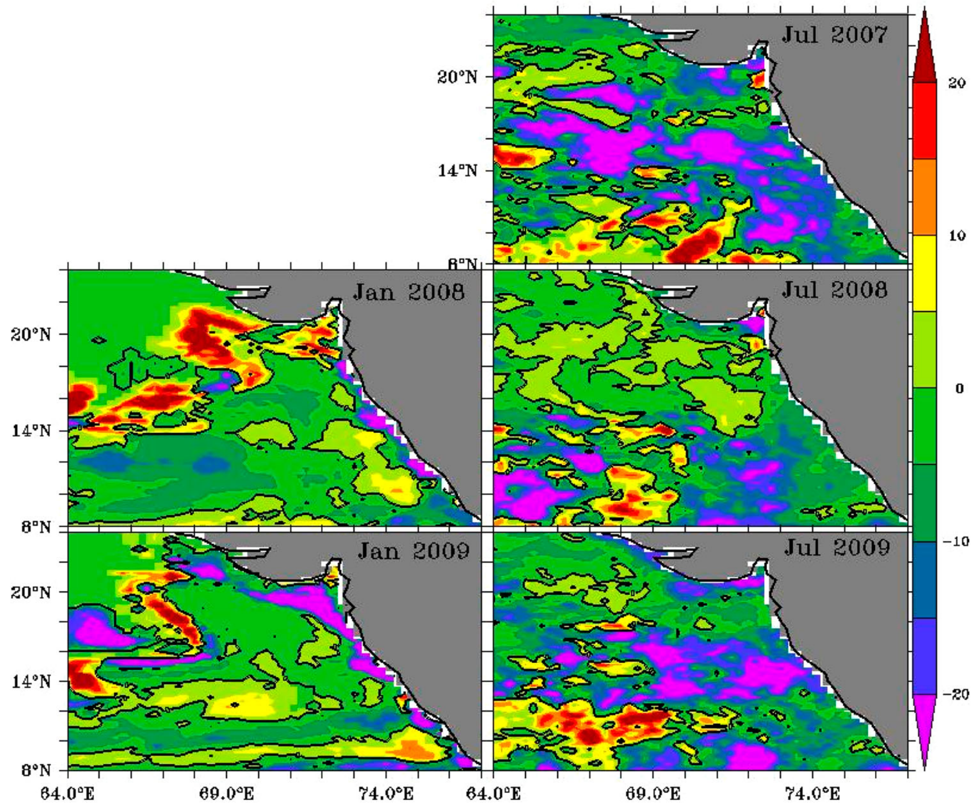

Figure 5. Difference in model-simulated depth (m) of chlorophyll maxima ${}_{ChlMax}D$ between QuickSCAT and ASCAT wind-forcings (i.e. ${}_{ChlMax}D^{QSCAT}$ − ${}_{ChlMax}D^{ASCT}$) from EAS for summer monsoon (July) and winter monsoon (January) of 2007–2009.

(January–March) is another governing process that triggers phytoplankton blooms, but it is generally located north of 20°N and west of 67°E which is beyond the selected sub-region. The *in situ* stations in this sub-region are highly scattered with very few points on the shelf, while offshore stations were away from the bloom region, mostly located within 18–20°N (Figure 1). However, the sub-region is indeed influenced by lateral advection of seasonal blooms, which being a remote contributor may not have direct correlation with wind-forcing in the simulation. Nevertheless, it can be inferred that the wind influence on sub-region's productivity is the least among all three.

Although the sub-region is mainly influenced by the advective blooms of winter convective mixing, its signature was prominently seen in the year 2008. In this year, SCM_{Depth} reached to the surface (Figure 4), which is a usual phenomenon. Whereas in 2009, the deeper SCM_{Depth} at ∼30 m with magnitude nearly half of 2008 maximum was mainly attributed to the strong El-Niño and positive Indian Ocean Dipole (IOD) conditions (Cai et al. 2009); when the resultant warm upper water column had been associated with weak convective mixing and less blooms. This confirms that our model had performed well in responding to the global processes which are least-dependent to the regional wind-induced effects.

4.3.2. CEAS

For CEAS there were fewer observations available (Figure 1) and most of them were underestimated by model simulations (Figure 6). After applying a preset threshold of ±90% bias in QuickSCAT and ASCAT outputs, 54 and 58 data-points remained, respectively (Figure 6). Similar to the correlation obtained for NEAS, QuickSCAT forcing yielded better correlation when compared to ASCAT forcing. While systematic bias (intercept) and slope were better in the case of the ASCAT forced model, correlation in terms of RMSE value indicated better performance by QuickSCAT forcing.

4.3.3. SEAS

There were few but major overestimations observed in SEAS (Figure 6). The magnitude of overestimation here was maximum in all the three sub-regions. However, often these ambiguities arise due to model simulating the chlorophyll maxima at a depth different from the observed chlorophyll maxima. As it had been in the other sub-regions, in SEAS majority observations were

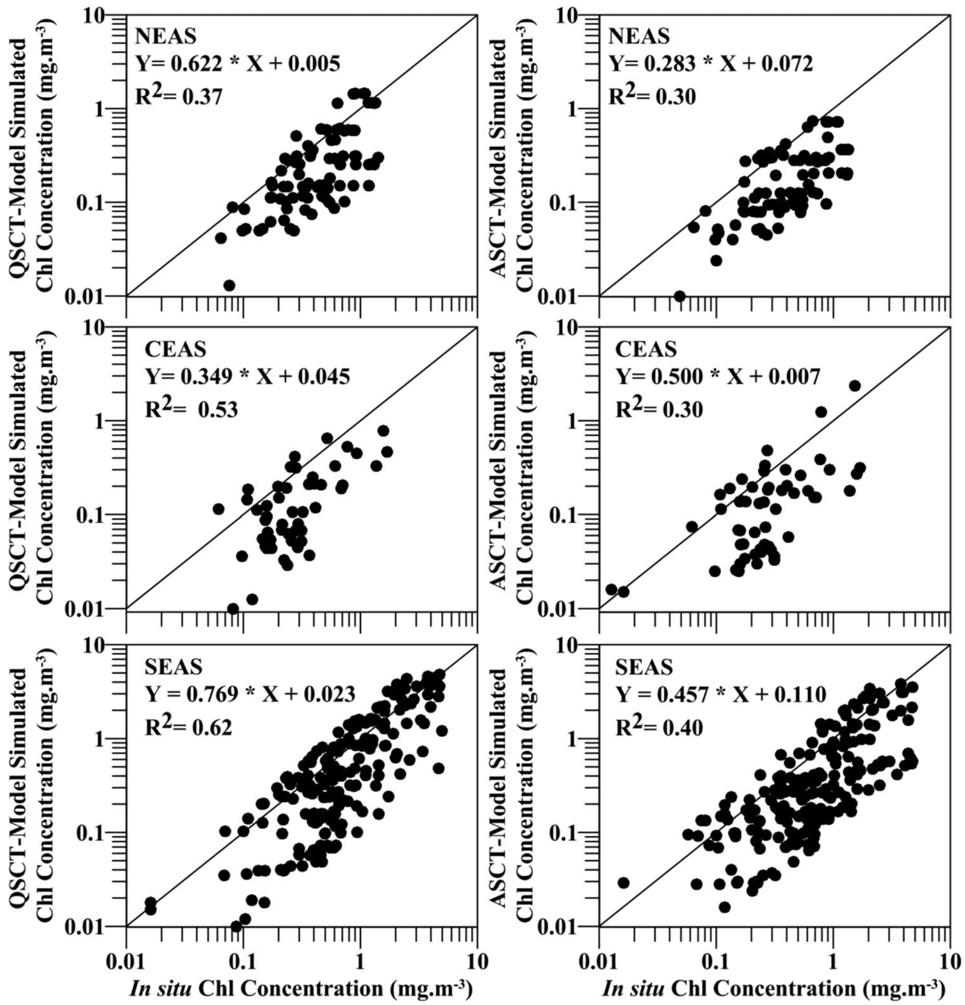

Figure 6. Correlation between *in situ* chlorophyll concentration and wind-forced model outputs (after applying QC threshold of ±90% bias) for the sub-regions along the EAS.

the cases of underestimation by the model and that trend persisted for both of the forcings. The trend as well as the magnitude of bias were also similar between the forcing sources.

For SEAS, observations with chlorophyll values higher than 5 mg m^{-3} were flagged and not used for comparison, as exceeding these values are generally seen only up to inner shelf (~30 km from the coast) during summer upwelling (Gupta et al. 2016) and dynamics of which is only possible to capture by employing a higher resolution model than the one we used here. Similar flagging was also applied to the model outputs with >5 mg m^{-3} chlorophyll concentrations. Upon applying a threshold of ±90% bias in QuickSCAT and ASCAT forced model outputs, 198 and 210 data-points remained, respectively, which was the maximum among all three sub-regions. Like other regions, SEAS also exhibited the best correlation with respect to QuickSCAT ouput with *in situ* data (Figure 6). Noticeably, this correlation was maximum with QuickSCAT ($R^2 = 0.62$) and minimum with ASCAT outputs ($R^2 = 0.40$) among all three regions. The highest number of observations within this shelf (Figure 1), together with wide variation in correlations between these wind-forcing outputs, infers that wind influence on upwelling in this region is quite significant in which QuickSCAT forced model simulations performed better than ASCAT forcing.

Overall, QuickSCAT wind-fields were able to force the model more efficiently and thus generated more realistic simulation for the coastal EAS. In this regard, we infer that zones with negative values in Figure 5 (ASCAT forced model yielding deeper chlorophyll maxima) are the regions where ASCAT wind-fields underperformed significantly.

4.4. Comparison with satellite data

In addition to validate our model outputs with *in situ* observations, we also attempted comparison with satellite data. Presently, satellite data are the only source that provide large-scale spatial (e.g. basin-wide) and temporal (daily, throughout the year) data coverage, which no other mechanisms can provide. On the other hand, a model that captures variability at the scales similar to satellite data can also provide insights to sub-surface processes. Additionally, such a model will have forecasting capabilities which satellite data lack. To achieve this, we extracted eight-day average surface chlorophyll concentrations from the model simulations spatially averaged over the sub-regions (Figure 1). We compared these to the chlorophyll concentration data of SeaWiFS and MODIS-Aqua satellite, averaged at the same spatio-temporal resolution to that of the model outputs.

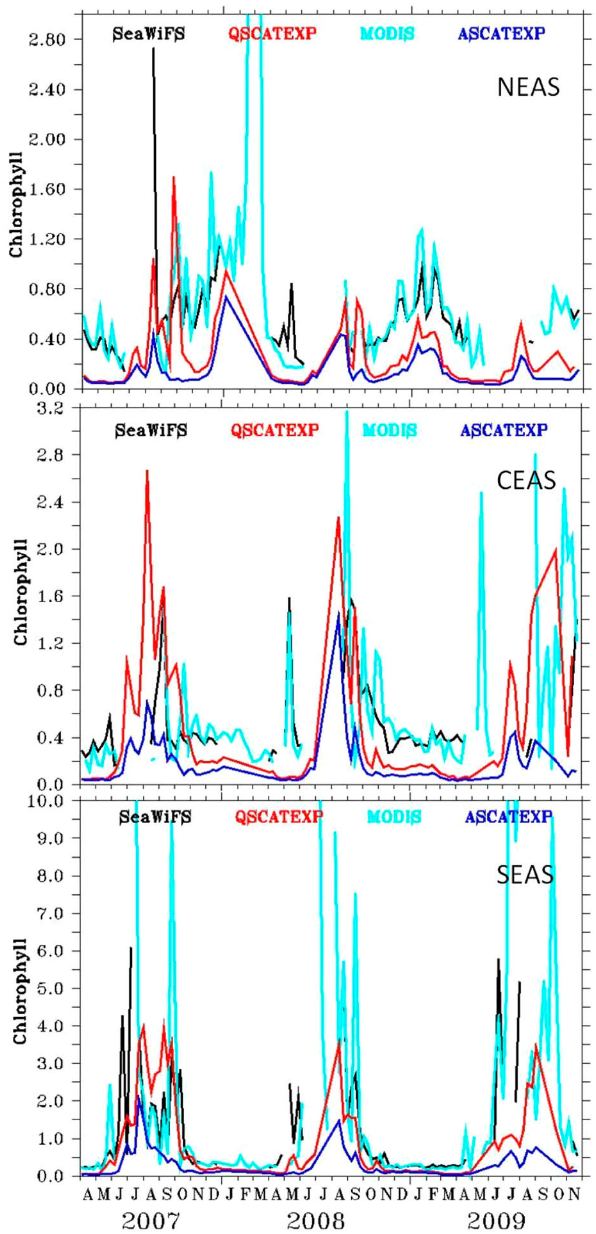

Figure 7. Comparison of spatially averaged time-series chlorophyll concentrations (mg m^{-3}) derived from model simulations (respective forcings as in colour legends) with that derived from SeaWiFS and MODIS-Aqua satellite data, for NEAS, CEAS and SEAS (upper, middle and lower panels, respectively) during 2007–2009.

In general, the model results followed the satellite chlorophyll trend but magnitude-wise they are relatively close to SeaWiFS especially during blooming phases. The QuickSCAT forced model induced relatively high degree of wind-induced mixing or upwelling. This resulted in higher entrainment of nutrients into mixed layer leading to high surface chlorophyll concentrations (Figure 7). It is to be noted that satellite estimated chlorophyll concentrations are integrated over the column up to first optical depth (FOD) which is a function of water clarity. This means even though the length of integration varies significantly, universal and reliable determination of the FOD as a number is not possible with the present technology. Also, chlorophyll concentration is a spatially discrete parameter. In the numerical simulation of biophysical ocean models, the upper ocean layer tends to behave as a homogenous system. Due to these conditions, when the chlorophyll concentration is averaged spatially over a large area such as in this study, differences between remote sensing observation and model simulation are expected. This is amplified especially during short events that lead to spike in high concentrations. However, we observed that the model could capture much of the variability that was related to the seasonality.

In the NEAS, the model captured the time-series trend well in comparison to SeaWiFS and MODIS-A derived chlorophyll concentration (Figure 7). However, model outputs were of lower magnitude in comparison to the satellite data during most of the simulation period. This is expected due to limitation in satellite-derived data as explained above. With FOD data, it is possible to integrate model output to the same depths which we believe can provide comparable results to satellite data. However, during ISM (≈JJAS), the model outputs were overestimating chlorophyll when compared to the satellites data (Figure 7). This was most significant for the year 2007. A possible reason for such bias could be that the photosynthetically active/available radiation (PAR) information provided to the model is a climatology data product. So, when the PAR conditions are anomalously low, the model may still allow more light to be available for photosynthesis. For a region such as NEAS that witness usually short monsoon compared to other two regions, monsoon in the year 2007 was active above-average due to La Niña conditions that lead to prolonged cloud cover and higher rainfall. Extended cloud cover tends to hamper the productivity temporarily by reducing light availability. Assimilation of monthly PAR values instead of climatology can provide realistic light availability to the euphotic zone. This could lead to corrected photosynthetic rates. Such course-correction can reduce the differences between observations and simulations.

Similar trends were observed in model simulations for CEAS and SEAS which appear to have followed closely with SeaWiFS data despite data gaps especially during blooming periods of 2008 and 2009 (Figure 7). Overall, the MODIS detected chlorophyll peaks were much larger than both the wind-induced model simulations. *Trichodesmium* spp bloom is a recurrently occurring phenomenon in these regions during April–May (Jabir et al. 2013; Gupta et al. 2016). These are atmospheric N-fixing cyanobacteria, which supply nitrogen to the ocean and proliferate under calm, warm and oligotrophic (N depleted) conditions (Gupta et al. 2016; Stanley 2016). While satellite captures this bloom models failed under both the wind-fields. Although the model captures such favourable environmental conditions, it failed to trigger the bloom as the model used is yet to be improved to simulate species succession and eventual draw-down of atmospheric N.

There appears to have phase lag in chlorophyll peaks between model outputs and satellite data in CEAS and SEAS. While model detected peaks in early to mid-monsoon (June–August) satellite, especially MODIS, did the same to the extended periods up to October (Figure 7). The upwelling of nutrient-replete waters reach surface in these regions by May which combines with nutrient influx from monsoon-fed rivers and supported proliferation of blooms (Gupta et al. 2016). While upwelling dissipates after August in the SEAS, its continued existence even after late summer monsoon in the CEAS, together with the availability of nutrients discharged from monsoonal rivers continue to support phytoplankton production even after monsoon retreats (Dileep Kumar 2011; Sudheesh et al. 2016). However, the present model is trained only to entrain nutrients from the below mixed layer through upwelling and detected corresponding peaks of chlorophyll and the model is not subjected to surface run-off parameters due to lack of data required for the same. As a result, the model not only underestimated chlorophyll during peak monsoon but also could not resolve peaks for the extended period at which satellites did. Overall, the model has simulated chlorophyll trends well in accordance to the satellite data although it underperformed in terms of magnitude due to the constraints as discussed above.

4.5. Potential causes for the differences in the forcings

Inherently, ASCAT and QuickSCAT sensors are differently conceptualised and designed. QuickSCAT had larger swath and shorter revisit time in comparison to ASCAT (Schlax et al. 2001). QuickSCAT data were also available closer to the shore than ASCAT which results in better ground coverage. It is reported that QuickSCAT also had lower relative errors between 20° and 30°N latitudes (Schlax et al. 2001). However, scatterometers basically operate by observing wind-driven surface waves. Temperature influences viscosity of the ocean surface layer and affects more negatively the QuickSCAT performance than that of ASCAT during low wind conditions (less than 3 m s^{-1}), the reverse is true during high-wind conditions with ASCAT (Bentamy et al. 2008, 2012). In order to perturb column properties, numerical models such as ours rely on advection forced through surface currents. Ocean currents are the end result of gradient in dynamic topography and Ekman transfer of mass triggered by wind-fields. Hence, it is important to have suitable wind-fields in order to simulate below-surface variability, for which the utility of QuickSCAT is known (Bourassa et al. 2010).

The northern Indian Ocean is the only part of the global oceans that has a spatial extent within the tropics. Additionally, it is characterised with distinct monsoon seasons. Raindrops are known to attenuate and backscatter microwave signal with which scatterometers operate. Higher frequencies (i.e. smaller wavelengths) are affected more by the larger size of raindrops (Portabella and Stoffelen 2001). This was the case of QuickSCAT which operated at a higher frequency (12–18 GHz or Ku-Band) than ASCAT which operated at the C-band (5.255 GHz). Our study area is dominated by coastal processes, where Ekman pumping largely defines the structural properties of the water column. Thus, the forcing as well as data availability nearer to the coastline from QuickSCAT provide better simulations.

In this regard, comparison of both sensors' performance shows that the derived wind-fields are in agreement with observations from buoys (Sivareddy et al. 2013). It has also been reported that for open ocean surface currents, remote forcing of high-wind episodes at the equatorial Indian Ocean is better simulated with QuickSCAT forcing (Ravichandran et al. 2013; Sivareddy et al. 2015).

5. Conclusion

This paper provides an important case study of wind-forcing sensitivity analysis to the numerical ocean modelling for the AS. The performance of wind-fields derived from two prominent satellite-based scatterometer sensors – QuickSCAT and ASCAT – has been compared for the overlapping window of two years in their operations. Our findings show that even though ASCAT has proven its usefulness in providing wind-observations comparable to its predecessors and to the *in situ* observations; data gaps arising from two narrow parallel swaths yield errors when forcing a biophysical model such as ROMS with its gap-free derivative (Schlax et al. 2001). In advancement with the previous modelling studies for this region, we conclude that this is a prime limitation to the utility of ASCAT data in development of operational modelling and forecasting capabilities. This can be solved by choosing a sensor design that is similar to QuickSCAT while resolving wind-calculation errors from the presence of raindrops. Alternatively, multiple satellites carrying ASCAT type sensors can be deployed, in order to minimise data gaps in the merged final product.

Multi-lateral efforts are being taken up by international scientific community to study the Indian Ocean, especially the basins of the northern Indian Ocean – for applications ranging widely from fishery resource management to weather research and forecasting (George et al. 2010; Hyder et al. 2012). These efforts heavily rely on satellite as well as model simulations for deeper understanding of the column properties, as well as oceanic processes. This study aims to help adding present knowledge in setting up a model for one of these basins – the AS – that intend to provide products spanning the duration which encounter scatterometer transition. Dynamics of thermocline and its association with sub-surface chlorophyll maxima due to nutrient entrainment can provide vertical extent of upper ocean productivity. Fishery oceanographers and policy-makers of this region need tools to study and manage the resources effectively. Primary and secondary productivity estimation with the help of a model such as this can be immensely helpful. Better estimation of detritus export to the deeper waters can help estimations of carbon sink. Trigger for sudden outbreaks of bloom can be studied efficiently. This may also enhance our knowledge on dynamics of OMZs and capacity on forecasting the same. Basin-wide gap-free data for multiple years from the model can also aid in studying teleconnection of El Niño–Southern Oscillation and IOD to the biogeochemistry of the basin. Another area of study that may benefit from the model is impact of extreme events on the marine ecology of the region.

Acknowledgements

KC wishes to acknowledge use of the ROMS software in simulating the state of the ocean and use of the Ferret program for analysis in this paper. KC earnestly thanks HOOFS team members for the help in setting up the ROMS simulations. KC acknowledges the DMG group and CWG Group of INCOIS, respectively, for providing bio-Argo data and necessary support to run ROMS in INCOIS-HPC. KC gratefully acknowledges the Director, INCOIS for his encouragement and unconditional help. We thank NOAA CoastWatch Program, NASA-GSFC and IFREMER (Institut français de recherche pour l'exploitation de la mer) for providing data used in this study. We also thank Sanjiba Kumar Baliarsingh for helping us in modifying a figure. We are grateful to Arya Paul for critically carrying out internal review of the draft. This is INCOIS and CMLRE contribution nos. 302 and 85, respectively.

Disclosure statement

No potential conflict of interest was reported by the authors.

Funding

The ecosystem model configured as a part of High-resolution Operational Ocean Forecasting and reanalysis System (HOOFS) programme coordinated by the Indian National Centre for Ocean Information Services (INCOIS) and funded by Ministry of Earth Sciences (MoES) [Ref: MoES/36/OOIS/HOOFS/2012].

ORCID

Kunal Chakraborty http://orcid.org/0000-0001-6940-9355
Nimit Kumar http://orcid.org/0000-0002-3815-5919
G. V. M. Gupta http://orcid.org/0000-0003-1437-9034

References

Amol P, Shankar D, Aparna SG, Shenoi SS, Fernando V, Shetye SR, Mukherjee A, Agarvadekar Y, Khalap S, Satelkar NP. 2012. Observational evidence from direct current measurements for propagation of remotely forced waves on the shelf off the west coast of India. J Geophys Res Oceans. 117(C5). doi:10.1029/2011JC007606.

Bentamy A, Croize-Fillon D, Perigaud C. 2008. Characterization of ASCAT measurements based on buoy and QuikSCAT wind vector observations. Ocean Sci. 4 (4):265–274.

Bentamy A, Fillon DC. 2012. Gridded surface wind fields from Metop/ASCAT measurements. Int J Remote Sens. 33 (6):1729–1754.

Bentamy A, Grodsky SA, Carton JA, Croizé-Fillon D, Chapron B. 2012. Matching ASCAT and QuikSCAT winds. J Geophys Res Oceans. 117(C2). doi:10.1029/2011JC007479.

Bourassa M, Bonekamp H, Chang P, Chelton D, Courtney J, Edson R, Figa J, He Y, Hersbach H, Hilburn K, et al. 2010. Remotely sensed winds and wind stresses for marine forecasting and ocean modeling. Proc Ocean Obs. 9.

Burillo IA, Caniaux G, Gavart M, De Mey P, Baraille R. 2002. Assessing ocean-model sensitivity to wind forcing uncertainties. Geophys Res Lett. 29(18):5-1–5-4.

Cai W, Pan A, Roemmich D, Cowan T, Guo X. 2009. Argo profiles a rare occurrence of three consecutive positive Indian Ocean Dipole events, 2006–2008. Geophys Res Lett. 36(8). doi:10.1029/2008GL037038.

Chakraborty K, Gupta A, Lotliker AA, Tilstone G. 2016. Evaluation of model simulated and MODIS-aqua retrieved

sea surface chlorophyll in the eastern Arabian Sea. Estuar Coast Shelf Sci. 181:61–69.
Chapman DC. 1985. Numerical treatment of cross-shelf open boundaries in a barotropic coastal ocean model. J Phys Oceanogr. 15(8):1060–1075.
Chauhan OS, Raghavan BR, Singh K, Rajawat AS, Kader U, Nayak S. 2011. Influence of orographically enhanced SW monsoon flux on coastal processes along the SE Arabian Sea. J Geophys Res Oceans. 116(C12). doi:10.1029/2011JC007454.
Devol AH, Uhlenhopp AG, Naqvi SWA, Brandes JA, Jayakumar DA, Naik H, Gaurin S, Codispoti LA, Yoshinari T. 2006. Denitrification rates and excess nitrogen gas concentrations in the Arabian Sea oxygen deficient zone. Deep Sea Res Pt I Oceanogr Res Papers. 53(9):1533–1547.
Dileep Kumar M. 2011. Nitrogen in the north Indian Ocean. In: Raghuram N, editor. ING bulletins on regional assessment of reactive nitrogen. Bulletin No. 10. New Delhi: SCON-ING; p. i–iv & 1–23.
Fennel K, Wilkin J, Levin J, Moisan J, O'Reilly J, Haidvogel D. 2006. Nitrogen cycling in the Middle Atlantic Bight: results from a three-dimensional model and implications for the North Atlantic nitrogen budget. Global Biogeochem Cycles. 20(3). doi:10.1029/2005GB002456.
Flather RA. 1976. A tidal model of the northwest European continental shelf. Mem Soc R Sci Liege. 10(6):141–164.
George MS, Bertino L, Johannessen OM, Samuelsen A. 2010. Validation of a hybrid coordinate ocean model for the Indian Ocean. J Oper Oceanogr. 3(2):25–38.
Gupta GVM, Sudheesh V, Sudharma KV, Saravanane N, Dhanya V, Dhanya KR, Lakshmi G, Sudhakar M, Naqvi SWA. 2016. Evolution to decay of upwelling and associated biogeochemistry over the southeastern Arabian Sea shelf. J Geophys Res Biogeosci. 121:159–175.
Habeebrehman H, Prabhakaran MP, Jacob J, Sabu P, Jayalakshmi KJ, Achuthankutty CT, Revichandran C. 2008. Variability in biological responses influenced by upwelling events in the eastern Arabian Sea. J Marine Syst. 74:545–560.
Haidvogel DB, Arango H, Budgell WP, Cornuelle BD, Curchitser E, Di Lorenzo E, Fennel K, Geyer WR, Hermann AJ, Lanerolle L, et al. 2008. Ocean forecasting in terrain-following coordinates: formulation and skill assessment of the regional ocean modeling system. J Comput Phys. 227(7):3595–3624.
Hyder P, Storkey D, Blockley E, Guiavarc'h C, Siddorn J, Martin M, Lea D. 2012. Assessing equatorial surface currents in the FOAM global and Indian Ocean models against observations from the global tropical moored buoy array. J Oper Oceanogr. 5(2):25–39.
Jabir T, Dhanya V, Jesmi Y, Prabhakaran MP, Saravanane N, Gupta GVM, Hatha AAM. 2013. Occurrence and distribution of a diatom-diazotrophic Cyanobacteria association during a Trichodesmium bloom in the southeastern Arabian Sea. Int J Oceanogr. doi:10.1155/2013/350594.
Jayaram C, Chacko N, Joseph KA, Balchand AN. 2010. Interannual variability of upwelling indices in the Southeastern Arabian Sea: a satellite based study. Ocean Sci J. 45(1):27–40.
Joshi M, Rao AD. 2012. Response of southwest monsoon winds on shelf circulation off Kerala Coast, India. Cont Shelf Res. 32:62–70.
Keen TR, Kindle JC, Young DK. 1997. The interaction of southwest monsoon upwelling, advection and primary production in the northwest Arabian Sea. J Marine Syst. 13(1–4):61–82.
Large WG, McWilliams JC, Doney SC. 1994. Oceanic vertical mixing: a review and a model with a nonlocal boundary layer parameterization. Rev Geophys. 32(4):363–403.
Lisan Y, Jin X, Weller RA. 2008. Multidecade global flux datasets from the objectively an analyzed air-sea fluxes (OAFlux) project: latent and sensible heat fluxes, ocean evaporation, and related surface meteorological variables. OAFlux Project Technical Report OA-2008-01.
Madhupratap M, Gopalakrishnan TC, Haridas P, Nair KKC. 2001. Mesozooplankton biomass, composition and distribution in the Arabian Sea during the fall intermonsoon: implications of oxygen gradients. Deep Sea Res Pt II Topical Stud Oceanogr. 48(6):1345–1368.
Maltrud ME, McClean JL. 2005. An eddy resolving global 1/10 ocean simulation. Ocean Model. 8(1):31–54.
Menon HB, Lotliker A, Nayak SR. 2005. Pre-monsoon bio-optical properties in estuarine, coastal and Lakshadweep waters. Estuar Coast Shelf Sci. 63(1–2):211–223.
Menon HB, Lotliker AA, Moorthy KK, Nayak SR. 2006. Variability of remote sensing reflectance and implications for optical remote sensing – a study along the eastern and northeastern waters of Arabian Sea. Geophys Res Lett. 33 (15):857.
Menon HB, Sangekar NP, Lotliker AA, Vethamony P. 2011. Dynamics of chromophoric dissolved organic matter in Mandovi and Zuari estuaries – a study through in situ and satellite data. ISPRS J Photogramm Remote Sens. 66 (4):545–552.
Naqvi SWA, Jayakumar DA, Narvekar PV, Naik H, Sarma VVSS, D'souza W, Joseph S, George MD. 2000. Increased marine production of N_2O due to intensifying anoxia on the Indian continental shelf. Nature. 408(6810):346–349.
Parsons T, Takahashi M, Hargrave B. 1984. Biological oceanographic processes. 3rd ed. Oxford: Pergamon Press, p. 330.
Penny SG, Behringer DW, Carton JA, Kalnay E. 2015. A hybrid global ocean data assimilation system at NCEP. Mon Weather Rev. 143(11):4660–4677.
Pickard GL, Emery WJ. 1990. Descriptive physical oceanography: an introduction. Pergamon: Elsevier.
Portabella M, Stoffelen A. 2001. Rain detection and quality control of SeaWinds. J Atmos Ocean Tech. 18(7):1171–1183.
Prakash P, Prakash S, Rahaman H, Ravichandran M, Nayak S. 2012. Is the trend in chlorophyll-a in the Arabian Sea decreasing? Geophys Res Lett. 39(23). doi:10.1029/2012GL054187.
Prasanna Kumar S, Ramaiah N, Gauns M, Sarma VVSS, Muraleedharan PM, Raghukumar S, Dileep Kumar M, Madhupratap M. 2001 Physical forcing of biological productivity in the northern Arabian Sea during the Northeast Monsoon. Deep Sea Res. Pt II. 48:1115–1126.
Preusser F, Radies D, Matter A. 2002. A 160,000-year record of dune development and atmospheric circulation in southern Arabia. Science. 296(5575):2018–2020.
Qasim SZ. 2003. Indian Estuaries 259 pp. Mumbai: Allied.
Raghavan BR, Deepthi T, Ashwini S, Shylini SK, Kumarswami M, Kumar S, Lotliker AA. 2010. Spring inter monsoon algal blooms in the eastern Arabian sea: shallow marine

encounter off Karwar and Kumbla coast using a hyperspectral radiometer. Int J Earth Sci Eng. 3(6):827–832.
Rao PG, Al-Sulaiti M, Al-Mulla AH. 2001. Winter Shamals in Qatar, Arabian Gulf. Weather. 56(12):444–451.
Rao PG, Hatwar HR, Al-Sulaiti MH, Al-Mulla AH. 2003. Summer shamals over the Arabian Gulf. Weather. 58 (12):471–478.
Ravichandran M, Behringer D, Sivareddy S, Girishkumar MS, Chacko N, Harikumar R. 2013. Evaluation of the global ocean data assimilation system at INCOIS: the Tropical Indian Ocean. Ocean Model. 69:123–135.
Ravichandran M, Girishkumar MS, Riser S. 2012. Observed variability of chlorophyll-a using Argo profiling floats in the southeastern Arabian Sea. Deep Sea Res Pt I Oceanogr Res Papers. 65:15–25.
Sarma VVSS, Kumar MD, George MD. 1998. The central and eastern Arabian Sea as a perennial source of atmospheric carbon dioxide. Tellus B Chem Phys Meteorol. 50(2):179–184.
Sarupria JS, Bhargava RMS. 1993. Seasonal primary production in different sectors of the EEZ of India. Mahasagar. 26:139–147.
Schlax MG, Chelton DB, Freilich MH. 2001. Sampling errors in wind fields constructed from single and tandem scatterometer datasets. J Atmos Ocean Tech. 18(6):1014–1036.
Shetye SR, Gouveia AD, Singbal SY, Naik CG, Sundar D, Michael GS, Nampoothiri G. 1995. Propagation of tides in the Mandovi-Zuari estuarine network. Proc Indian Acad Sci Earth Planet Sci. 104(4):667–682.
Shetye SR, Shenoi SSC. 1988. Seasonal cycle of surface circulation in the coastal north Indian Ocean. Proc Indian Acad Sci Earth Planet Sci. 97(1):53–62.
Shulman IG, Kindle JC, DeRada S, Anderson SC, Penta B. 2003. Development of a hierarchy of nested models to study the California current system (No. NRL/PP/7330-03-20). Naval Research Lab Stennis Space Center MS Oceanography DIV.
Sindhu B, Suresh I, Unnikrishnan AS, Bhatkar NV, Neetu S, Michael GS. 2007. Improved bathymetric datasets for the shallow water regions in the Indian Ocean. J Earth Syst Sci. 116(3):261–274.
Singh RP, Prasad AK, Kayetha VK, Kafatos M. 2008. Enhancement of oceanic parameters associated with dust storms using satellite data. J Geophys Res. 113:2296. doi:10.1029/2008JC004815
Sivareddy S, Ravichandran M, Girishkumar MS. 2013. Evaluation of ASCAT-based daily gridded winds in the tropical Indian Ocean. J Atmos Ocean Tech. 30(7):1371–1381.
Sivareddy S, Ravichandran M, Girishkumar MS, Prasad KV. 2015. Assessing the impact of various wind forcing on INCOIS-GODAS simulated ocean currents in the equatorial Indian Ocean. Ocean Dynamics. 65(9–10):1235–1247.
Srinivas K, Dineshkumar PK. 2006. Atmospheric forcing on the seasonal variability of sea level at Cochin, southwest coast of India. Cont Shelf Res. 26:1113–1133.
Stanley S. 2016. An unprecedented view of biogeochemistry off India's west coast. EOS. 97. doi:10.1029/2016EO046753
Sudheesh V, Gupta GVM, Sudharma KV, Naik H, Shenoy DM, Sudhakar M, Naqvi SWA. 2016. Upwelling intensity modulates N_2O concentrations over the western Indian shelf. J Geophys Res Oceans. 121:8551–8565.
Sudre JCM, Garçon V. 2013. On the global estimates of geostrophic and Ekman surface currents. Limnol Oceanogr Meth. 3:1–20.
Tilstone GH, Lotliker AA, Miller PI, Ashraf PM, Kumar TS, Suresh T, Ragavan BR, Menon HB. 2013. Assessment of MODIS-aqua chlorophyll-a algorithms in coastal and shelf waters of the eastern Arabian Sea. Cont Shelf Res. 65:14–26.
Webster PJ, Moore AM, Loschnigg JP, Leben RR. 1999. Coupled ocean–atmosphere dynamics in the Indian Ocean during 1997–98. Nature. 401(6751):356–360.
Zeebe RE, Wolf-Gladrow DA. 2001. CO_2 in seawater: equilibrium, kinetics, isotopes. Vol. 65. Houston, TX: Gulf Professional Publishing.